

Article

Analyzing SPIF Product Characteristics Using Full Factorial Design-Integrated PCA Approach

Adham E. Ragab 

Department of Industrial Engineering, College of Engineering, King Saud University, P.O. Box 800, Riyadh 11421, Saudi Arabia; aragab@ksu.edu.sa

Abstract: The process of single-point incremental forming (SPIF) is a relatively new technology that is primarily used in the production of prototypes and small quantities of products. However, the process has several limitations with respect to the quality characteristics of its products. This study examined the effects of four process parameters—namely, tool diameter, feed rate, step size, and sheet thickness—on the characteristics of the final product. A total of 15 product responses were measured and/or calculated during the experiments. The responses fell under three different categories; surface profile accuracy, strain/stress/thinning, and forming forces. In previous published work, responses were studied separately for each category. The aim of this paper was to determine the relationships between responses using a principal component analysis (PCA). PCA is a well-known multivariate analysis technique used to reduce the dimensionality of data. As a result of the PCA, the product's characteristic dimensions were reduced from 15 while 71% of the total variance of data was preserved. The results showed that only 8 responses were enough to characterize the final product, rather than 15. A relationship was detected between the side wall accuracy and forming forces and between strain, circularity, and surface roughness. These findings could not be detected with single-variable analyses.

Keywords: SPIF; PCA; profile accuracy; forming force; principal strain



Citation: Ragab, A.E. Analyzing SPIF Product Characteristics Using Full Factorial Design-Integrated PCA Approach. *Processes* **2023**, *11*, 1254. <https://doi.org/10.3390/pr11041254>

Academic Editor: Antonino Recca

Received: 19 February 2023

Revised: 6 April 2023

Accepted: 18 April 2023

Published: 19 April 2023



Copyright: © 2023 by the author. Licensee MDPI, Basel, Switzerland. This article is an open access article distributed under the terms and conditions of the Creative Commons Attribution (CC BY) license (<https://creativecommons.org/licenses/by/4.0/>).

1. Introduction

Incremental sheet forming (ISF) is a relatively new technology used primarily to produce prototypes and small batches of products. In this regard, the process is economically advantageous as it permits the production of complex shapes of thin sheet metal without the use of a special die. Compared with traditional sheet metal processes, this process offers a number of advantages, including lower initial costs, shorter lead times, enhanced formability limits, and greater process flexibility [1]. The process does have some limitations due to the poor quality of its final product's surface, non-uniform thickness distribution of the parts, and the long forming time required compared with other competitive sheet metal processes.

The concept of sheet forming with a single-point tool was patented by Leszak in 1967, long before it was technically feasible [1,2]. Several industries have used the process recently, including automobiles, aerospace industries, biomedical applications, and appliances [3]. There are two main types of ISF; single-point incremental forming (SPIF) and two-point incremental forming (TPIF). TPIF differs from SPIF in that it includes a supporting die underneath the sheet workpiece [4]. A general-purpose CNC milling machine is used in both categories, and with a simple generic tool, several products of different complex geometries can be made directly from their CAD models.

In order to study ISF processes, a wide range of practical issues had to be addressed and resolved. Several researchers were concerned with the accuracy of the geometric properties of the product, including dimensional errors [5,6], waviness [4], and side wall angle errors [7]. Design of experiments (DOE) was employed to assess the effect of different process parameters on the accuracy of the produced profile, including the response surface

method (RSM) [6,8], Taguchi [9], and factorial design [10]. Many ISF research activities have also addressed the issue of surface roughness, such as [11–13]. In addition, researchers have examined the strain and thinning of workpieces; for example [14–17].

As the number of studied responses increases, researchers tend to use multivariate analyses. In this way, they are able to gain a deeper understanding of the relationships between these variables. There have been a few studies conducted in the field of ISF that have applied a multivariate analysis. In their study, Chinnaiyan et al. used a Taguchi-based grey relational analysis (GRA) coupled to a PCA to find the combination of seven forming parameters that optimized the SPIF formability of an AA5052 sheet [3]. In this study, surface roughness and formability, presented as the sum of major strain and minor strain, were measured. The suggested hybrid optimizing technique resulted in enhancing the formability and surface roughness by 56% and 93%, respectively.

Raju et al. employed a Taguchi-based GRA in conjunction with the response surface method (RSM) to optimize formability, wall angle, forming time, surface finish, and springback parameters [18]. The suggested hybrid technique could predict the optimal combination of five process parameters; namely, tool diameter, feed rate, spindle speed, number of sheets, and vertical step depth. Validating experiments resulted in an improvement of 1.42% in the grey grade value.

This study examined four process parameters in order to determine their impact on final product characteristics; namely, tool diameter, feed rate, step size, and sheet thickness. A total of 15 product responses were measured and/or calculated during the experiment. There were three categories of responses; these were the profile accuracy and surface roughness, sheet straining, and forming forces. In previous publications [19–21], responses were studied in separate categories.

To investigate the relationships among the 15 responses, a multivariate analysis was used in this paper. For the purpose of this study, the PCA was chosen as a method of reducing the dimensionality of the data and achieving a simple structure while retaining most of the original data variance. To the best of the author's knowledge, a multivariable analysis has not been used in SPIF to analyze these different categories of part characteristics. The results of this paper allowed a reduction in the needed measurements to characterize the final product, hence reducing the cost of such quality control tests.

2. Materials and Methods

2.1. Experiment Setup

The aluminum alloy used in this study was commercial aluminum alloy AA 1050-H14. This material was selected for its common availability and low cost. The chemical composition of the sheet, listed in Table 1, was determined by a SPECTROMAXx machine, model LMF05 36 (AMETEK, Kleve, Germany). A Zwick/Roell universal testing machine was used to carry out tensile tests on the specimens according to the ASTM standards. Table 2 shows the mechanical properties of the samples.

Table 1. Chemical composition of AA 1050-H14 sheets.

Sample	Al %	Fe %	Si %	Ti %	Other
1	99.5	0.368	0.0480	0.0216	0.0624
2	99.5	0.360	0.0496	0.0205	0.0007

Table 2. Mechanical properties of aluminum alloy AA 1050-H14.

Material Code	Yield Strength σ_y (MPa)	Ultimate Tensile Strength σ_{UTS} (MPa)	Elongation at Break	Young Modulus E (MPa)
AA1050-H14	108	117.5	8.45%	67,648

To achieve the objective of this study, a simple part was designed in the shape of a truncated cone with a height of 50 mm and a base diameter of 100 mm, as shown in Figure 1b,d. A special fixture was designed and manufactured to be used on a vertical CNC milling machine. To allow a free deformation of the workpiece under the applied load, dedicated fixtures were designed from three separate parts. Initially, the workpiece was a square sheet with 240 mm sides and the working area was 200×200 mm. Figure 1a illustrates the setup of the fixture and the machine.

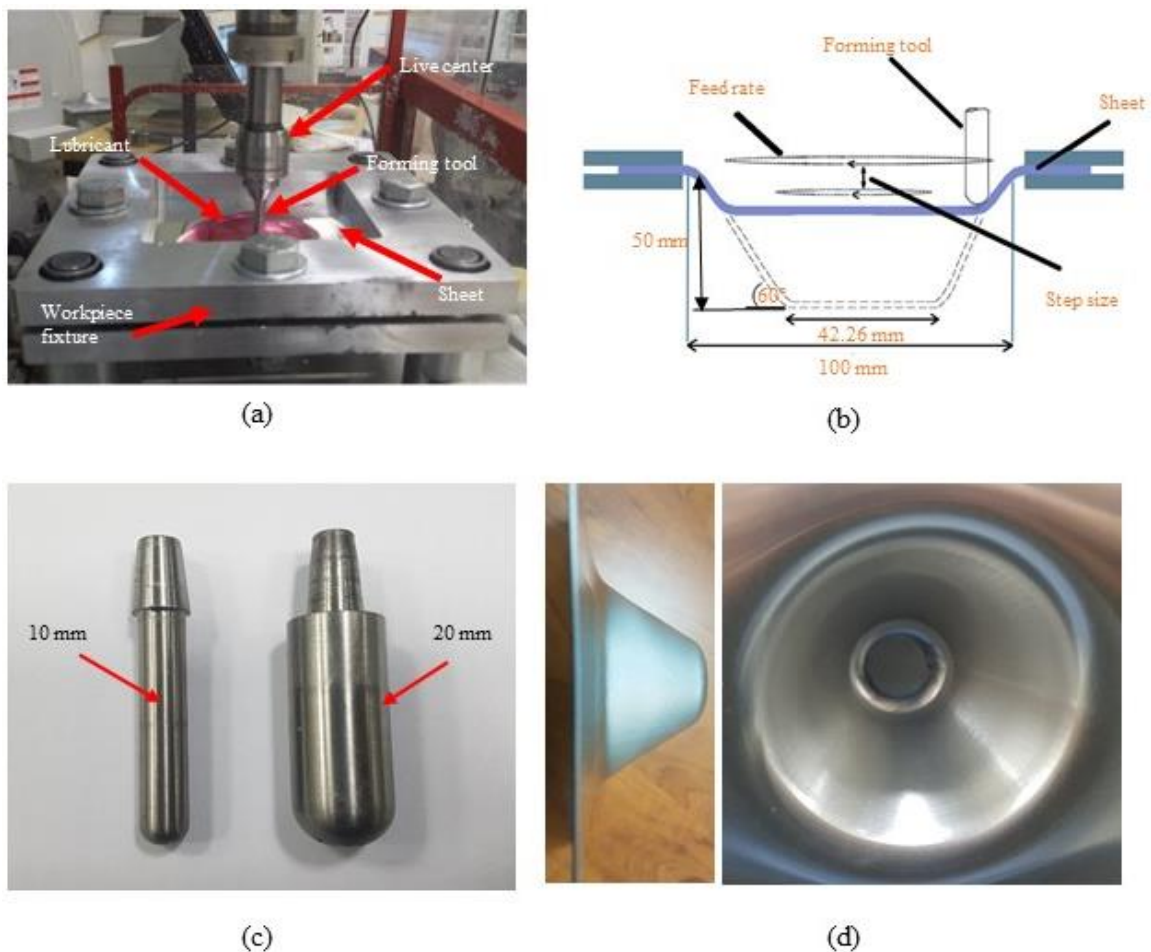


Figure 1. (a) Fixture and machine setup, (b) part dimensions and the investigated process parameters, (c) forming tools, and (d) final part.

Figure 1b shows a schematic drawing of the process depicting the part geometry, forming tool, feed rate direction, and vertical step. Figure 1c shows the tool geometry with two different diameters. Hardened D2 steel was used to make the forming tools. The hemispherical tip of the tool was polished in order to reduce friction with the workpiece. The tool was attached to a live center so it could rotate freely. The machine spindle did not rotate during the experiments and lubricating oil was utilized to minimize friction.

In order to fabricate a given product, several tool paths may be used. In this study, a spiral tool path, generated by MASTERCAM software, was used. The tool contours were created using the transition step method [22]. During the manufacture of the part, the tool formed one circle, and then moved down the step size in accordance with the program. In this manner, the process was repeated until the part was fully fabricated. Along the formed circles, the tool moved at a constant speed equal to the preset feed rate.

The experimental design matrix was generated using a full factorial design with four factors (controllable process parameters) and two levels for each factor. There were two replications of each experiment. Table 3 presents the four factors, along with their levels.

The studied process parameters were chosen due to their expected effects on the final product [5–17]. Preliminary experiments were used to determine their levels. With the current setup, factor values beyond the selected levels resulted in flawed parts.

Table 3. Process parameters and their levels.

Annotation	Process Parameter (Factor)	Low Level	High Level
TD	Tool diameter (mm)	10	20
FR	Feed rate (mm/min)	500	1000
SS	Step size (mm)	0.5	1
ST	Sheet thickness (mm)	1	2

2.2. Measurements

2.2.1. Force Measurement

The forming force in three directions was measured with a KISTLER 2825A1 force dynamometer located under the fixture. A KISTLER 5019B amplifier was connected to the dynamometer for signal amplification. With these apparatuses, the forming forces applied to the part by the tool were recorded at a sampling rate of 50 Hz using a data acquisition system [19].

2.2.2. Profile Accuracy Measurement

There were four types of profile accuracy items that were considered [21]; namely, the circularity error, waviness error, side angle error, and part depth error. To estimate the four profile errors mentioned above, a Zeiss ACCURA CMM with an accuracy of 2 μm was used. Approximately 300 points were detected on each produced part using a 3 mm probe.

Throughout the depth of the cone, circularity errors were estimated at three different levels. The CMM was used to measure the coordinates of 30 points along a circular path in the XY-plane while maintaining a constant probe height in the z-direction. The process was repeated at locations C1, C2, and C3, as shown in Figure 2a. A typical circularity error test exhibited a circular deviation, as shown in Figure 2b. For each level of measurement (C1, C2, and C3), a circle was fitted using the least squares method and the maximum radial deviations (inside and outside the fitted circle) were recorded (B1 and B2). Based on ISO 230 4:2005(E) [23], the circularity error was calculated as the maximum radial separation between two concentric circles enclosing the actual path. The circularity error was calculated as the sum of the two deviations, B1 and B2.

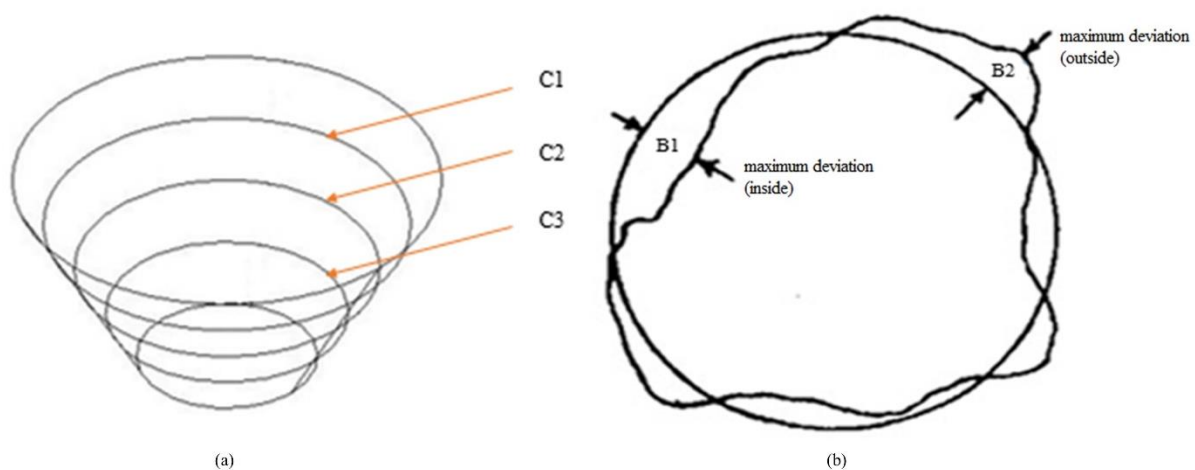


Figure 2. Circularity error: (a) level of circular path in XY-plane; (b) circularity deviation.

Due to the variable diameter along the depth of the part, the circularity error was normalized with respect to the nominal diameter of the part. The normalized circularity errors were referred to as NC1, NC2, and NC3, respectively, and were defined by the circularity error/nominal diameter of the part.

The waviness error was determined by selecting approximately 200 points along 4 paths (W1, W2, W3, and W4), as shown in Figure 3a. The recorded points were used to fit a line using the least squares method. This process was repeated along each of the four paths that were 90° apart. Figure 3b shows the maximum deviations from the line (A1 and A2). According to ASME B46.1-1985 [24], the waviness deviation is calculated as the sum of A1 and A2. Using two values, the waviness error is expressed as the average and maximum of each part's four deviations.

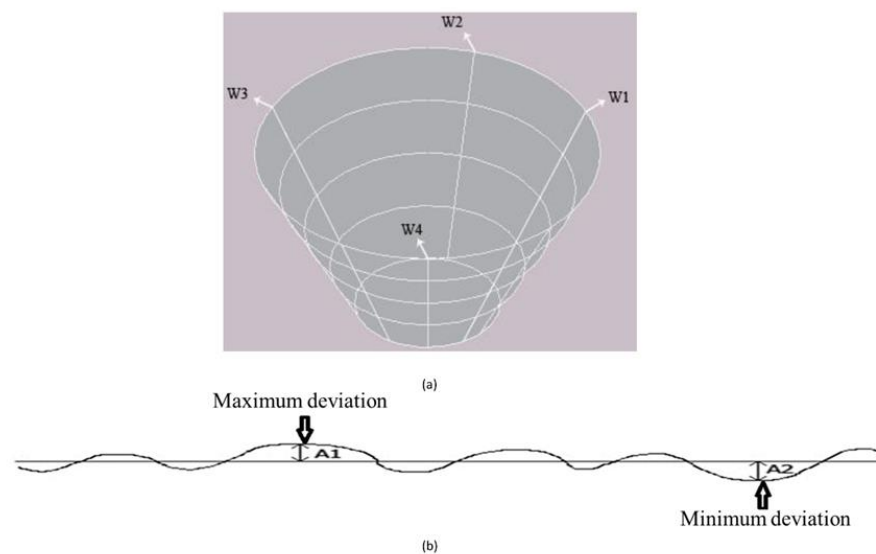


Figure 3. (a) Surface waviness paths and (b) maximum and minimum deviation along path.

The side angle is the angle formed by the side walls of parts with respect to the horizontal XY-plane, as shown in Figure 1b. The side angle error is defined as the difference between the actual and designed side angle (60°).

The part depth was determined by measuring the distance between the top and bottom of the cone. The error was calculated as the difference between the actual and designed depth of the part (50 mm).

2.2.3. Measuring Strain

A grid of squares with a side length of 2 mm was electrochemically etched onto the surface of the workpiece before forming in order to measure the strains and calculate the stresses and thinning of the final part, as shown in Figure 4. In order to determine the strains and calculate the stresses and thinning, a grid analyzer, model 100 (FMTI Systems, Ontario, Canada) was utilized. Strain was measured at various points along the wall to capture the variation in the wall. The measurements were taken along lines L1, L2, and L3, with five grids being selected on each line, as shown in Figure 4b. Principal stresses were calculated from the experimental values of principal strains by the GRID ANALYZER using the following equation:

$$\sigma = c\varepsilon^n$$

where the constant (C) = 146.9 and strain hardening exponent (n) = 0.3. Details regarding this procedure may be sought in [21].

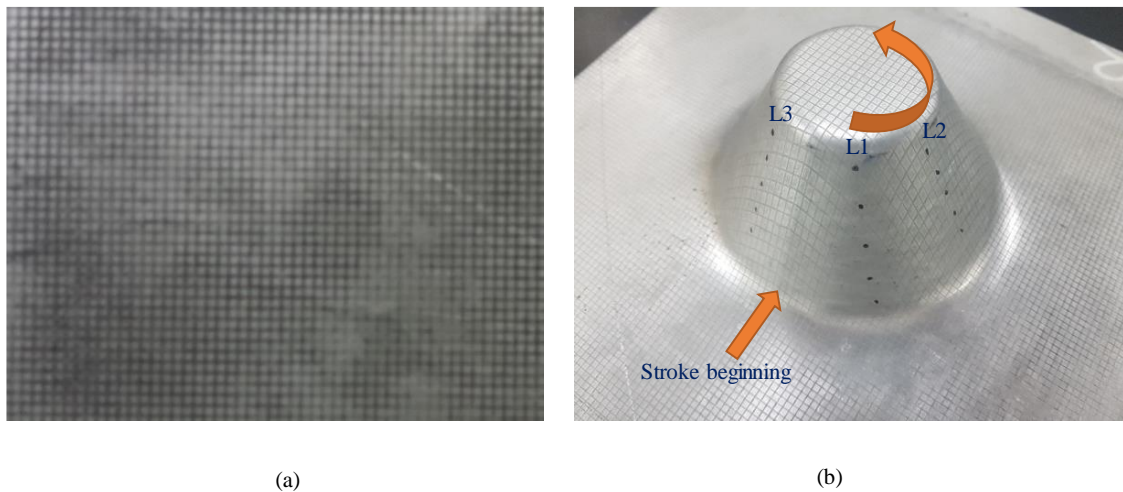


Figure 4. (a) Initial sheets etched with 2 mm square grid pattern; (b) sheet after deformation with measurement locations.

2.2.4. Measuring Roughness

Ra and Rt were measured at four locations on the part's inner surface and each measurement was repeated twice. As a measure of surface roughness, the average of both the Ra and Rt measurements was recorded for each part. Measurements were conducted using 0.8 mm cut-offs and 4 mm evaluation lengths.

2.3. Principal Component Analysis (PCA)

The PCA method is an unsupervised technique widely used in exploratory data analyses [25]. The primary objective of a PCA is to reduce data dimensionality with a minimum loss of information in order to enhance interpretability. In this technique, the original data are projected onto a series of orthogonal components (called principal components or PCs) in such a way as to maximize the variance captured by these components [26]. PCs are linear combinations of the original variables with different loadings, which represent the amount that each variable contributes to a particular PC.

Every PC carries a higher percentage of data variance than the one preceding it, which is a critical feature of a PCA. While the number of calculated PCs is the same as the number of original variables, this property allows the selection of a few PCs, beginning with PC1. As a result, the data can be represented in a reduced number of dimensions. To determine the optimal number of PCs to include in an analysis, several criteria have been proposed [25,26]. According to Kaiser's criterion (average eigenvalue criterion), PCs are significant only if their eigenvalue exceeds the average eigenvalue, which is 1 when the data are scaled. Alternatively, a cut-off percentage of cumulative variance can be established and only PCs that meet this threshold are considered. In general, the cut-off point ranges between 70 and 90% [27].

3. Results and Discussion

A summary of the studied factors and the measured or calculated responses is presented in Table 4. According to a previous section, the factors that were examined were the tool diameter, the feed rate, the step size, and the sheet thickness. The surface profile response variables included normalized circularity (NC1, NC2, and NC3), average and maximum waviness (AW and MW (mm)), side angle error (AE (°)), depth error (DE (mm)), and surface roughness parameters (Ra and Rt (μm)). In terms of deformation behavior response variables, maximum principal strain (MPST), maximum principal stress (MPS (MPa)), and maximum thinning (MT) were measured. The force response variables included maximum force in the z-direction (Fz), maximum force in the x-direction (Fx), and maximum force in the y-direction (Fy). All force values were measured in KN.

Table 4. Experimental plan and responses.

Serial	TD mm	FR mm/min	SS mm	ST mm	NC1	NC2	NC3	AW mm	MW mm	AE Degrees	DE mm	Ra μm	Rt μm	MPST	MPS MPa	MT	Fz KN	Fx KN	Fy KN
1	20	1000	0.5	2	0.061	0.072	0.098	0.52	0.84	0.93	0.92	0.55	5.25	0.82	163	0.58	1.60	0.70	0.69
2	10	500	1	1	0.058	0.070	0.095	0.38	0.56	−1.31	1.42	1.75	15.63	0.81	162	0.57	0.43	0.29	0.27
3	20	500	1	2	0.059	0.074	0.097	0.73	1.26	1.00	0.78	0.68	8.75	0.81	163	0.59	1.67	0.99	0.86
4	10	500	1	1	0.061	0.077	0.107	0.50	0.81	0.88	−0.73	2.10	20.25	0.84	163	0.57	0.53	0.32	0.33
5	20	500	0.5	2	0.061	0.076	0.098	0.54	0.96	0.75	1.85	0.55	7.38	0.83	165	0.62	1.42	0.72	0.71
6	10	500	1	2	0.060	0.063	0.101	0.53	0.88	1.66	−1.89	2.08	17.88	0.72	156	0.55	1.49	0.83	0.87
7	20	500	0.5	1	0.059	0.078	0.095	0.39	0.67	−0.47	0.92	0.40	3.75	0.97	172	0.64	0.49	0.32	0.31
8	10	1000	0.5	1	0.051	0.072	0.098	0.34	0.48	0.03	−0.55	1.98	18.88	0.79	161	0.58	0.38	0.23	0.22
9	20	1000	0.5	1	0.056	0.073	0.094	0.40	0.68	−0.41	0.91	0.43	5.00	0.87	161	0.57	0.69	0.32	0.34
10	10	1000	1	2	0.058	0.073	0.104	1.01	1.45	1.17	−1.99	2.30	19.38	0.74	158	0.56	1.58	0.78	0.89
11	10	500	0.5	1	0.057	0.073	0.106	0.43	0.81	−0.05	−1.63	1.40	15.75	0.76	160	0.59	0.46	0.20	0.21
12	10	1000	0.5	2	0.059	0.074	0.110	0.99	1.46	0.40	−1.66	2.10	16.75	0.73	157	0.55	1.29	0.57	0.55
13	10	500	0.5	1	0.059	0.078	0.103	0.43	0.78	−0.03	−1.56	1.45	14.25	0.77	158	0.54	0.43	0.20	0.20
14	20	1000	1	2	0.051	0.075	0.097	0.94	1.42	1.13	0.69	0.65	8.50	0.82	162	0.58	1.76	0.87	0.90
15	20	500	0.5	2	0.054	0.068	0.094	0.48	0.77	0.96	1.51	0.60	6.63	0.86	165	0.6	1.64	0.78	0.77
16	20	1000	0.5	2	0.053	0.079	0.097	0.61	0.95	0.61	0.95	0.53	5.63	0.86	165	0.59	1.64	0.68	0.71
17	10	1000	0.5	1	0.058	0.073	0.095	0.33	0.67	−0.42	−0.91	2.30	19.88	0.76	158	0.57	0.38	0.19	0.19
18	20	500	0.5	1	0.061	0.072	0.096	0.35	0.56	−0.16	2.38	0.58	5.75	0.97	174	0.66	0.52	0.32	0.32
19	10	500	1	2	0.060	0.069	0.110	0.85	1.46	0.38	−2.01	1.98	18.88	0.74	158	0.56	0.72	0.38	0.38
20	20	1000	1	1	0.054	0.064	0.100	0.68	1.48	0.68	1.64	0.40	4.00	0.8	162	0.58	0.67	0.37	0.38
21	10	500	0.5	2	0.049	0.074	0.098	0.93	1.49	0.60	−1.46	2.35	19.38	0.7	155	0.55	1.26	0.51	0.54
22	10	1000	0.5	2	0.050	0.072	0.096	0.97	1.38	0.32	−1.45	2.50	18.63	0.73	156	0.55	0.47	0.20	0.24
23	10	1000	1	2	0.057	0.076	0.102	0.83	1.16	1.00	−1.81	1.88	14.75	0.72	157	0.56	0.56	0.26	0.27
24	20	1000	1	2	0.059	0.074	0.098	0.75	1.19	1.07	0.69	0.70	11.13	0.84	164	0.59	1.63	0.86	0.87
25	20	500	1	1	0.059	0.075	0.100	0.49	0.76	0.86	0.60	0.40	3.88	0.87	164	0.58	0.28	0.17	0.17

Table 4. Cont.

Serial	TD mm	FR mm/min	SS mm	ST mm	NC1	NC2	NC3	AW mm	MW mm	AE Degrees	DE mm	Ra μm	Rt μm	MPST	MPS MPa	MT	Fz KN	Fx KN	Fy KN
26	20	1000	0.5	1	0.054	0.068	0.090	0.35	0.46	0.16	1.74	0.43	4.50	0.98	172	0.63	0.53	0.31	0.30
27	20	500	1	1	0.054	0.074	0.103	0.40	0.56	0.12	1.83	0.40	3.63	0.84	164	0.59	0.24	0.16	0.16
28	20	1000	1	1	0.055	0.075	0.104	0.42	0.74	0.11	1.72	0.43	4.63	0.89	167	0.61	0.22	0.14	0.14
29	20	500	1	2	0.051	0.076	0.102	0.92	1.33	0.79	0.67	0.90	12.13	0.86	165	0.58	0.87	0.42	0.45
30	10	1000	1	1	0.060	0.065	0.095	0.43	0.65	0.35	−0.33	2.03	15.88	0.86	165	0.59	0.54	0.25	0.25
31	10	1000	1	1	0.056	0.076	0.097	0.59	0.88	−0.09	−1.49	1.88	16.63	0.78	161	0.59	0.18	0.11	0.11
32	10	500	0.5	2	0.056	0.074	0.099	0.85	1.33	0.78	−1.42	2.25	20.25	0.72	156	0.54	0.47	0.22	0.26

As the data are presented on different scales, normalized values are used in a PCA [28]. It is possible to accomplish this by using a correlation matrix rather than a covariance matrix in the analysis. As the correlation coefficient between two variables is calculated by dividing their covariance with the product of their standard deviations, the values of the correlation matrix are normalized between -1 and $+1$. Table 5 presents the Pearson correlation matrix for all 15 response variables. In order to avoid adding redundant information to the analysis, it is recommended to avoid variables with high correlations [28]. It is assumed that the limit for a high correlation is when the Pearson correlation coefficient (r) equals 0.7 [29]. Consequently, if two response variables have $r > 0.7$, only one will be considered in the analysis. Regarding the Pearson values presented in Table 5, only the following variables were included in the analysis: NC1, NC2, NC3, AW, AE, Ra, MPST, and Fz.

Table 5. Pearson correlation for all response variables.

	NC1	NC2	NC3	AW	MW	AE	DE	Ra	Rt	MPST	MPS	MT	Fz	Fx
NC2	-0.055													
NC3	0.230	0.171												
AW	-0.296	0.124	0.362											
MW	-0.234	0.046	0.398	0.951										
AE	0.007	-0.105	0.239	0.537	0.535									
DE	-0.033	-0.028	-0.481	-0.450	-0.410	-0.184								
Ra	-0.016	-0.120	0.294	0.357	0.288	0.001	-0.855							
Rt	-0.000	-0.065	0.345	0.363	0.310	0.037	-0.850	0.968						
MPST	0.113	0.073	-0.457	-0.562	-0.583	-0.270	0.803	-0.750	-0.748					
MPS	0.152	0.060	-0.406	-0.525	-0.538	-0.229	0.805	-0.732	-0.722	0.969				
MT	0.153	0.040	-0.413	-0.513	-0.503	-0.242	0.734	-0.666	-0.659	0.859	0.935			
Fz	0.022	-0.048	-0.043	0.448	0.457	0.643	0.060	-0.151	-0.096	-0.135	-0.094	-0.072		
Fx	0.103	-0.096	-0.062	0.387	0.408	0.638	0.118	-0.194	-0.123	-0.071	-0.022	0.001	0.974	
Fy	0.068	-0.098	-0.041	0.432	0.443	0.667	0.072	-0.150	-0.084	-0.106	-0.062	-0.041	0.979	0.991

The rotation of the eigenvectors (components) was used to simplify the structure of the results; i.e., to achieve a condition in which the absolute value of variable loads near 1 or 0 on an eigenvector would allow for an easy interpretation of the factors [30]. There are two main types of rotation available in statistical software. Rotations can be either orthogonal or oblique, for which several methods are available. All rotation methods within the JASP software [31] were examined in this study. According to the output of the analysis, cluster rotation resulted in a structure that was closest to a perfect simple structure. According to the literature, if a perfect simple structure is not possible, cluster rotation performs better than other rotation methods [32]. For component loadings, a cut-off value of 0.4 was established to exclude those that were less than 0.4 because these were not considered salient [33].

In Figure 5, the scree plot illustrates the eigenvalues of the eight components after cluster rotation. Table 6 presents the eigenvectors, eigenvalues, and explained variation (contribution) for the first three components, where PC1, PC2, and PC3 represent the first three principal components after cluster rotation. There were only three components with eigenvalues greater than one, and thus they satisfied Kaiser's criterion. Furthermore, their cumulative contribution exceeded 0.714, which exceeded the cut-off limit of 0.7. As a result, only the first three components were considered in the rest of the analysis.

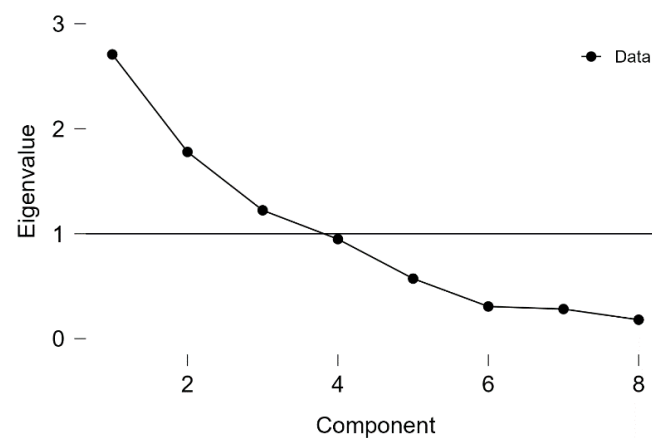


Figure 5. Scree plot of the eigenvalues.

Table 6. Eigenvectors, eigenvalues, and explained variation (contribution) for the first three PCs after cluster rotation.

	PC1	PC2	PC3
AE	0.899		
Fz	0.885		
AW	0.720		
Ra		0.931	
MPST		−0.814	
NC1		0.486	
NC2			0.876
NC3			0.659
Eigenvalue	2.267	2.168	1.274
Contribution	0.283	0.271	0.159
Cumulative	0.283	0.554	0.714

Figure 6 shows the path plot that related the original response variables to the three selected components PC1, PC2, and PC3. The principal components are shown on the left as circles. Variables are represented on the right by rectangles. A variable's loading on the principal components is represented by arrows pointing to the component. Red arrows indicate negative loadings and green arrows indicate positive loadings; the wider the arrow, the greater the loading.

PC1 was strongly influenced by the three variables AE, FZ, and AW, with all three pointing in a positive direction, as indicated in Table 6 and Figure 6. PC2 was controlled by Ra and NC1, which directed positive directions, and MPST, which directed negative directions. PC3 was controlled by the two variables NC2 and NC3, pointing in a positive direction.

Consequently, it was proposed that PC1 measured the side wall quality by relating the waviness error to the side angle error. As the forming force increased, PC1 suggested that the expected side wall quality decreased, both locally (waviness error) and generally (side angle error).

The interpretation of PC1 loadings indicated a causal relationship; however, those of PC2 did not appear to agree. There was generally a correlation between them, rather than a causal relationship. In general, the maximum principal strain, surface roughness, and circularity error at the top of the part were primarily influenced by the diameter of the tool [20,21]. The smaller the diameter of the tool, the greater the Ra and NC1 values, while the maximum principal strain was reduced. As a result, there was a negative correlation between them.

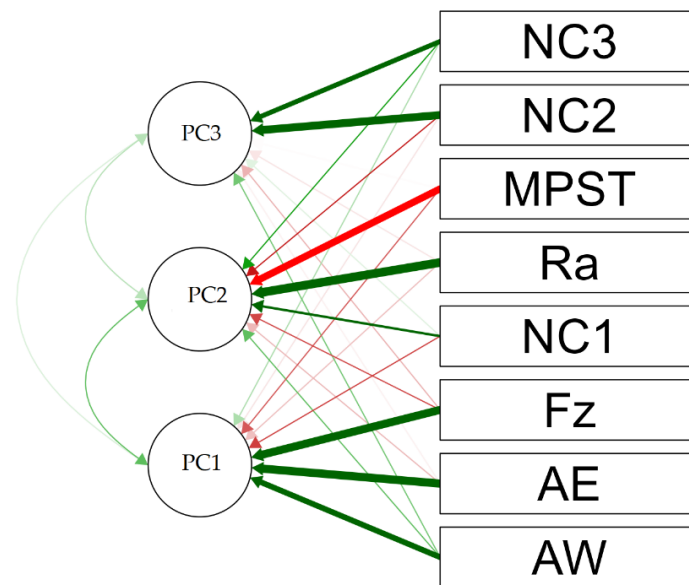


Figure 6. Path diagram for the first three PCs after cluster rotation.

PC3 represented the circularity errors at the middle and bottom of the part. Both of them progressed together as the springback increased with the depth of the part due to the increment of deformation in the sheet [20].

The score plots in Figure 7 show the results of the first two components, colored according to tool diameter (a), feed rate (b), step size (c), and sheet thickness (d). There is a clear distinction between the scores in Figure 7a,d as the scores divided into two regions whereas the scores in Figure 7b,c do not have this distinction. This was due to the fact that the tool diameter and sheet thickness had the greatest effect on the final product characteristics in this study.

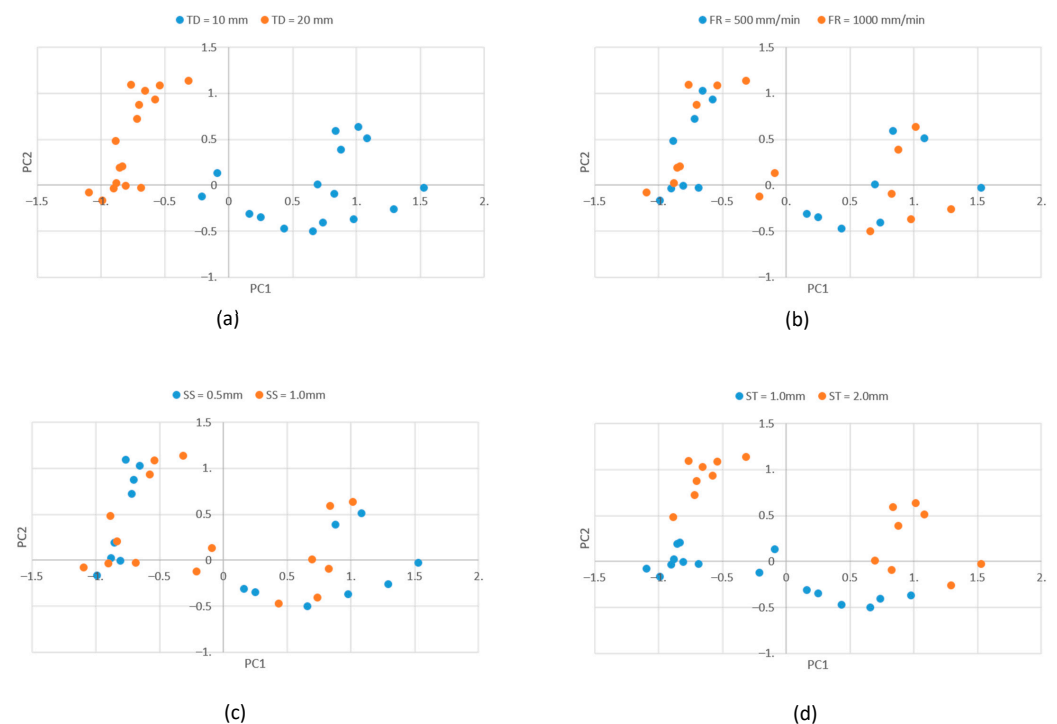


Figure 7. Score plot of the first two components colored by process parameter: (a) tool diameter; (b) feed rate; (c) step size; (d) sheet thickness.

In Figure 8, scores are presented in relation to both the tool diameter and sheet thickness at the same time. In the graph, there are four distinct regions that show a significant interaction between the tool diameter and sheet thickness. Research has previously demonstrated this interaction. As shown in the figure, sheet thickness separated the data around PC1 while the tool diameter separated the data around PC2. The sheet thickness had the greatest effect on the forming force [19] and, therefore, on the quality of the side walls, which was represented by PC1. In terms of surface roughness and principal strain, the tool diameter had the greatest impact [20,21].

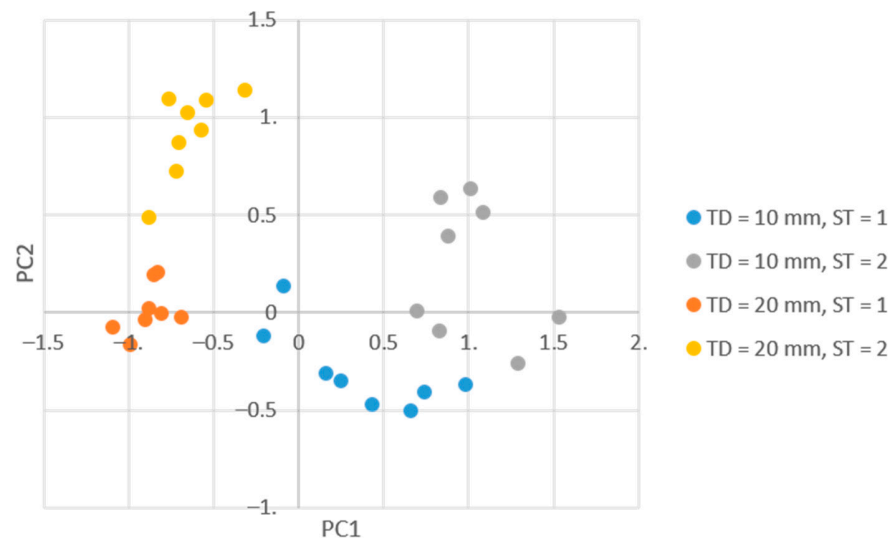


Figure 8. Score plot of the first two components colored by tool diameter and sheet thickness.

4. Conclusions

An exploratory study was conducted using SPIF to investigate the effect of four process parameters on the final product characteristics. A total of four process parameters were selected; namely, the diameter of the tool, the feed rate, the step size, and the thickness of the sheet. In order to construct the experiment matrix, a two-level full factorial design was utilized. For the final product, which was a simple truncated cone, 15 responses were measured/calculated. A total of three categories of responses were identified. These were (1) the surface profile accuracy; (2) the strains, stresses, and thinning; and (3) the forming forces. This response has previously been described as category-based in previous publications.

A PCA was used to uncover the relationships between the entire 15 responses. Based on a correlational analysis, only eight responses were sufficient to represent the product characteristics and the PCA was only performed on these eight responses. In order to create a close-to-perfect simple structure for the data, cluster rotation was applied. Cluster rotation resulted in the first three PCs representing all the studied responses while retaining 71% of the variance.

It has been suggested that the first component describes the side wall quality of the product (waviness error and side angle error) and that it should be combined with the forming force. It was concluded that a variation in the forming force was responsible for the side wall quality variation. Surface roughness, maximum principal strain, and normalized circularity at the top of the product were represented by PC2. It has been suggested that the correlation between the three responses was due to the fact that they were all primarily influenced by the same factors.

The main contribution of the results presented in this paper was the PCA's ability to reduce the number of measurements required to maintain the quality of the final SPIF product. Based on the relationship between waviness and angle errors, one could only measure one and conclude the other. It was also noteworthy that the product characteristics that were affected by the same process parameters behaved similarly, indicating that only

one of these characteristics needed to be examined, thereby reducing the cost of quality control. A single-variable analysis was not able to detect these findings.

The results presented in this paper provide a useful insight into the relationship between the various characteristics of SPIF products. By applying the same technique to different materials, product geometry, and process parameters, knowledge in this area can be deepened and its application expanded.

Funding: This research was funded by King Saud University, Researchers Supporting Project, number RSPD2023R711.

Data Availability Statement: We confirm that the experimental data used to support the findings of this study are included within the article.

Acknowledgments: The authors extend their appreciation to King Saud University for funding this work through Researchers Supporting Project, number RSPD2023R711, King Saud University, Riyadh, Saudi Arabia.

Conflicts of Interest: The authors declare no conflict of interest.

References

1. Jeswiet, J.; Micari, F.; Hirt, G.; Bramley, A.; Duflou, J.; Allwood, J. Asymmetric Single Point Incremental Forming of Sheet Metal. *CIRP Ann.* **2005**, *54*, 88–114. [\[CrossRef\]](#)
2. Leszak, E. Apparatus and Process for Incremental Dieless Forming. U.S. Patent US3342051A1, 19 September 1967.
3. Chinnaiyan, P.; Jeevanantham, A. Multi-Objective Optimization of Single Point Incremental Sheet Forming of AA5052 Using Taguchi Based Grey Relational Analysis Coupled with Principal Component Analysis. *Int. J. Precis. Eng. Manuf.* **2014**, *15*, 2309–2316. [\[CrossRef\]](#)
4. Attanasio, A.; Ceretti, E.; Giardini, C.; Mazzoni, L. Asymmetric Two Points Incremental Forming: Improving Surface Quality and Geometric Accuracy by Tool Path Optimization. *J. Mater. Process. Technol.* **2008**, *197*, 59–67. [\[CrossRef\]](#)
5. Ambrogio, G.; Costantino, I.; De Napoli, L.; Filice, L.; Fratini, L.; Muzzupappa, M. Influence of Some Relevant Process Parameters on the Dimensional Accuracy in Incremental Forming: A Numerical and Experimental Investigation. *J. Mater. Process. Technol.* **2004**, *153*, 501–507. [\[CrossRef\]](#)
6. Ambrogio, G.; Cozza, V.; Filice, L.; Micari, F. An Analytical Model for Improving Precision in Single Point Incremental Forming. *J. Mater. Process. Technol.* **2007**, *191*, 92–95. [\[CrossRef\]](#)
7. Petek, A.; Kuzman, K.; Kopač, J. Deformations and Forces Analysis of Single Point Incremental Sheet Metal Forming. *Arch. Mater. Sci. Eng.* **2009**, *35*, 107–116.
8. Hussain, G.; Lin, G.; Hayat, N. Improving Profile Accuracy in SPIF Process through Statistical Optimization of Forming Parameters. *J. Mech. Sci. Technol.* **2011**, *25*, 177–182. [\[CrossRef\]](#)
9. Kumar, N.; Belokar, R.M. Experimental Investigation of Geometric Accuracy in Single Point Incremental Forming Process of an Aluminium Alloy. *Int. J. Mater. Eng. Innov.* **2019**, *10*, 46–59. [\[CrossRef\]](#)
10. Ham, M.; Jeswiet, J. Single Point Incremental Forming and the Forming Criteria for AA3003. *CIRP Ann.* **2006**, *55*, 241–244. [\[CrossRef\]](#)
11. Kurra, S.; Rahman, N.H.; Regalla, S.P.; Gupta, A.K. Modeling and Optimization of Surface Roughness in Single Point Incremental Forming Process. *J. Mater. Res. Technol.* **2015**, *4*, 304–313. [\[CrossRef\]](#)
12. Mulay, A.; Ben, S.; Ismail, S.; Kocanda, A. Experimental Investigations into the Effects of SPIF Forming Conditions on Surface Roughness and Formability by Design of Experiments. *J. Braz. Soc. Mech. Sci. Eng.* **2017**, *39*, 3997–4010. [\[CrossRef\]](#)
13. Gulati, V.; Aryal, A.; Katyal, P.; Goswami, A. Process Parameters Optimization in Single Point Incremental Forming. *J. Inst. Eng. (India) Ser. C* **2016**, *97*, 185–193. [\[CrossRef\]](#)
14. Eyckens, P.; Belkassam, B.; Henrard, C.; Gu, J.; Sol, H.; Habraken, A.M.; Duflou, J.R.; Van Bael, A.; Van Houtte, P. Strain Evolution in the Single Point Incremental Forming Process: Digital Image Correlation Measurement and Finite Element Prediction. *Int. J. Mater. Form.* **2011**, *4*, 55–71. [\[CrossRef\]](#)
15. Yang, M.; Yao, Z.; Li, Y.; Li, P.; Cui, F.; Bai, L. Study on Thickness Thinning Ratio of the Forming Parts in Single Point Incremental Forming Process. *Adv. Mater. Sci. Eng.* **2018**, *2018*, 2927189. [\[CrossRef\]](#)
16. Giuliano, G.; Corrado, A.; Polini, W. A Geometric Algorithm to Evaluate the Thickness Distribution of Stretched Sheets through Finite Element Analysis. *Appl. Sci.* **2021**, *11*, 1905. [\[CrossRef\]](#)
17. Kumar, A.; Gulati, V. Optimization and Investigation of Process Parameters in Single Point Incremental Forming. *Indian J. Eng. Mater. Sci. (IJEMS)* **2021**, *27*, 246–255.
18. Raju, C.; Narayanan, C.S. Application of a Hybrid Optimization Technique in a Multiple Sheet Single Point Incremental Forming Process. *Measurement* **2016**, *78*, 296–308. [\[CrossRef\]](#)

19. Dabwan, A.; Ragab, A.E.; Saleh, M.; Daoud, A.K. Determining the Effect of Key Process Parameters on Forming Force of Single Point Incremental Sheet Metal Forming. In Proceedings of the International Conference on Industrial Engineering and Operations Management, Kuala Lumpur, Malaysia, 8–10 March 2016; pp. 2833–2840.
20. Dabwan, A.; Ragab, A.E.; Saleh, M.A.; Anwar, S.; Ghaleb, A.M.; Rehman, A.U. Study of the Effect of Process Parameters on Surface Profile Accuracy in Single-Point Incremental Sheet Forming of AA1050-H14 Aluminum Alloy. *Adv. Mater. Sci. Eng.* **2020**, *2020*, 7265941. [[CrossRef](#)]
21. Dabwan, A.; Ragab, A.E.; Saleh, M.A.; Ghaleb, A.M.; Ramadan, M.Z.; Mian, S.H.; Khalaf, T.M. Multiobjective Optimization of Process Variables in Single-Point Incremental Forming Using Grey Relational Analysis Coupled with Entropy Weights. *Proc. Inst. Mech. Eng. Part L J. Mater. Des. Appl.* **2021**, *235*, 2056–2070. [[CrossRef](#)]
22. Kalpakjian, S. *Manufacturing Processes for Engineering Materials*; Pearson Education: Noida, India, 1984; ISBN 81-317-0566-8.
23. ISO 230-4; Test Code for Machine Tools—Part 4: Circular Tests for Numerically Controlled Machine Tools. ISO: Geneva, Switzerland, 2008.
24. ASME B46. 1-1985; Surface Texture (Surface Roughness, Waviness and Lay). ASME: New York, NY, USA, 1995.
25. Ballabio, D. A MATLAB Toolbox for Principal Component Analysis and Unsupervised Exploration of Data Structure. *Chemom. Intell. Lab. Syst.* **2015**, *149*, 1–9. [[CrossRef](#)]
26. Dominguez, L.A.; Shokrani, A.; Flynn, J.; Dhokia, V.; Newman, S. Application of Multivariate Statistical Analysis for CNC Milling of Large Ti-6Al-4V Components. *Procedia Manuf.* **2019**, *38*, 800–807. [[CrossRef](#)]
27. Jolliffe, I.T. *Principal Component Analysis for Special Types of Data*; Springer: Berlin/Heidelberg, Germany, 2002; ISBN 0-387-95442-2.
28. Iezzoni, A.F.; Pritts, M.P. Applications of Principal Component Analysis to Horticultural Research. *HortScience* **1991**, *26*, 334–338. [[CrossRef](#)]
29. Mindrila, D.; Balentyne, P. Scatterplots and Correlation. Retrieved From 2017. Available online: https://www.westga.edu/academics/research/vrc/assets/docs/scatterplots_and_correlation_notes.pdf (accessed on 1 February 2023).
30. Corner, S. Choosing the Right Type of Rotation in PCA and EFA. *JALT Test. Eval. SIG Newsl.* **2009**, *13*, 20–25.
31. JASP Team. JASP (Version 0.17.1) [Computer software]. 2023. Available online: <https://jasp-stats.org/download/> (accessed on 30 January 2023).
32. Yamamoto, M.; Jennrich, R.I. A Cluster-based Factor Rotation. *Br. J. Math. Stat. Psychol.* **2013**, *66*, 488–502. [[CrossRef](#)] [[PubMed](#)]
33. Guadagnoli, E.; Velicer, W.F. Relation of Sample Size to the Stability of Component Patterns. *Psychol. Bull.* **1988**, *103*, 265–275. [[CrossRef](#)] [[PubMed](#)]

Disclaimer/Publisher’s Note: The statements, opinions and data contained in all publications are solely those of the individual author(s) and contributor(s) and not of MDPI and/or the editor(s). MDPI and/or the editor(s) disclaim responsibility for any injury to people or property resulting from any ideas, methods, instructions or products referred to in the content.